

Electrical resistivity and Hall effect in binary neutron-star mergers

Arus Harutyunyan¹, Antonios Nathanail¹, Luciano Rezzolla^{1,2}, and Armen Sedrakian^{2,1}

¹ Institute for Theoretical Physics, J. W. Goethe-University, Max-von-Laue Str. 1, D-60438 Frankfurt am Main, Germany

² Frankfurt Institute for Advanced Studies, Ruth-Moufang str. 1, D-60438 Frankfurt am Main, Germany

November 13, 2018

Abstract. We examine the range of rest-mass densities, temperatures and magnetic fields involved in simulations of binary neutron-star mergers and identify the conditions under which the ideal-magnetohydrodynamics approximation breaks down and hence the magnetic-field decay should be accounted for. We use recent calculations of the conductivities of warm correlated plasma in envelopes of compact stars and find that the magnetic-field decay timescales are much larger than the characteristic timescales of the merger process for lengthscales down to a meter. Because these are smaller than the currently available resolution in numerical simulations, the ideal-magnetohydrodynamics approximation is effectively valid for all realistic simulations. At the same time, we find that the Hall effect can be important at low densities and low temperatures, where it can induce a non-dissipative rearrangement of the magnetic field. Finally, we mark the region in temperature and density where the hydrodynamic description breaks down.

PACS. 97.60.Jd Neutron stars – 26.60.-c Nuclear matter aspects of neutron stars

1 Introduction

The recent detections of gravitational waves by the LIGO and Virgo detectors have opened a new chapter in multimessenger astronomy. Among these observations, the recent detection of a gravitational wave signal GW170817 originating from a binary neutron star (NS) inspiral [1] and a gamma-ray burst by the Fermi satellite GRB170817A [2], which were followed by electromagnetic counterparts [3, 4, 5, 6], has demonstrated the prominent role that binary neutron-star inspirals can play in astrophysics, particle physics, and cosmology [7].

The observations of GW170817 and GRB170817A provided the first direct evidence that a class of short gamma-ray bursts can be associated with the inspiral and merger of binary compact stars. As the magnetic field plays a central role in the generation of the GRBs, the physics of inspiral and merger of magnetized neutron stars can now be constrained directly by observations. The magnetohydrodynamics (MHD) simulations of these processes have advanced steadily over the recent past and the post-merger massive compact object can now be followed up to the point of collapse to a black hole over timescales of the order of tens of milliseconds; for reviews see, *e.g.*, [8, 9, 10]. General-relativistic simulations have been carried out in the ideal MHD limit (*i.e.*, with infinite-conductivity) by several groups [11, 12, 13, 14, 15, 16, 17] and a number of works have included the resistive (*i.e.*, finite conductivity) effects [18, 19, 20, 21].

The aim of this work is to investigate the conditions under which the non-ideal MHD effects can be important in the contexts of neutron star mergers and the evolution of the post-merger object. The motivation for doing so is three-fold. Firstly, the past resistive MHD simulations [18, 21] have used sim-

plified functional forms of conductivities aimed to provide a smooth interpolation between highly conducting core and low-conducting magnetosphere; these were independent of the temperature and composition of matter and were functions of its rest-mass density only. Finite-temperature, composition-dependent conductivities for relevant low-densities have become available recently [22] and will be used in our estimates below. Secondly, the relevance of the Hall effect which arises in anisotropically conducting plasma has not been assessed in the context of binary neutron star merger physics; for studies in the context of cold neutron stars see [23, 24]. We will show below that the Hall effect can play an important role in a certain density-temperature regime. Thirdly, the density-temperature regime where the MHD approximation breaks down and a kinetic description of plasma is needed has not been established so far.

The novel features of the post-merger remnant object have recently motivated a study of related transport properties of dense matter, such as thermal conduction and bulk and shear viscosities in the absence of electromagnetic fields [25]. On the basis of simple estimates supported by numerical simulations of non-dissipative merger and post-merger process, it was concluded that bulk viscous effects could be important. Along similar lines, here we will adopt a semi-analytical approach to estimate the various timescales with processes listed above, *i.e.*, Ohmic dissipation, Hall effect and breakdown of MHD. This will be supported by the results of *ideal* MHD simulations, which allow us to estimate the relevant scales of gradients of magnetic field components and density. These simulations validate the fact that the magnetic field gradients are much smaller than those for the density - a crucial underlying assumption of our semi-analytical analysis. Thus, our work is aimed at aiding

future dissipative MHD simulations in identifying the various physical regimes when realistic conductivities are employed.

This paper is organized as follows. In Sec. 2 we discuss the ideal MHD simulations of binary neutron star mergers. Section 3 collects the relevant formulae for the timescales involved. Our numerical results for the time- and lengthscales are presented in Sec. 4. Finally, our conclusions are given in Sec. 5.

2 Binary neutron-star merger simulations

The aim of this section is to discuss the relevant scales of magnetic field components and thermodynamical parameters in the simulations of magnetized binary neutron star mergers. As shown below the onset of the resistive MHD regime depends on the *resolution* of simulations, therefore we will, in addition, discuss this scale. In view of continuous progress in resolving smaller scales in the simulations, it is important to identify the scales at which the resistive MHD becomes mandatory irrespective of current computing capabilities. The current state of the art with respect to resolution is as follows.

The magnetic field in a merger process can be substantially amplified via the Kelvin-Helmholtz instability (KHI) [26]. The magnetorotational instability (MRI) [27, 28] can also take place in the post-merger object. Both instabilities are normally not captured at the typical resolutions of global simulations, that are limited to a grid resolution of the order of 100 – 200 m [29, 30, 31, 32, 33]. At the same time, simulations at ultra-high resolutions of 70 m [34] or even 12 m [16] struggle to describe the KHI in a convergent regime and hence determine reliably the actual magnetic-field amplification. Similarly, while less severe requirements are needed to capture the MRI [35, 16], the role played by parasitic instabilities in limiting the amplification of the magnetic field is still unclear [36]. Finally, the local shearing-box simulations of special-relativistic MHD turbulence seem to indicate that equipartition level magnetic field magnitudes could be reached [37, 38].

Let us now turn to the lengthscale over which significant variations of the magnetic field take place, which we denote as λ_B . Clearly, this lengthscale is bound from below by the resolution scale of any given simulation, l_0 , which was already mentioned just above. We note that the decay timescale of the magnetic field is proportional to the square of the lengthscale of variation of the magnetic field (see below), therefore it is limited from below by the spatial resolution used in the numerical simulation. Characteristic timescales of simulations also set the upper bound τ_0 over which the relevant quantities need to change to be relevant dynamically. The current highest resolution simulations of the merger process, which were aimed at a better resolution of the KHI and MRI and monitoring of magnetic field amplification [35, 39, 16], are limited in time after merger due to numerical costs. Lower-resolution simulations can be carried out up to the point of the collapse to a black hole or the formation of a differentially rotating and unstable neutron star, and last typically tens of milliseconds.

To extract the relevant lengthscales we used a simulation of the merger of an equal-mass magnetized binary neutron-star system with a total ADM mass of $M_{\text{ADM}} = 3.25M_\odot$ and initial orbital separation of 45 km. For the sake of reproducibility, we use the open-source Illinois GRMHD code [40] with the

finest resolution of $l_0 \approx 227$ m. Each star has a baryon mass of $1.625M_\odot$ and is endowed initially with a poloidal magnetic field fully contained inside the star. The maximum magnetic field in the initial configuration is a bit less than 10^{16} G and the merger takes place at $t_{\text{mg}} \approx 3.5$ ms after the start of the simulation.

For illustrative purposes, we show in Fig. 1 the rest-mass density (left panel) and the magnetic-field configuration (right panel) of the hypermassive neutron star (HMNS) created by the merger, at time $t - t_{\text{mg}} \sim 14.7$ ms. Similar behaviours are seen also at earlier and later times. Note that the rest-mass density of matter drops from nuclear saturation density down to $\rho \approx 10^{10}$ g cm $^{-3}$ over the lengthscale of 30 km, with sharp gradients at $z \approx 10$ and $x \approx 20$ km. Except for this transition region, the rest-mass density profile is smooth over the lengthscales of the order of several kilometres. In other words, an approximately constant rest-mass density can be considered when making estimates of quantities over lengthscales of the order of 10 km. This is shown in the lower part of the left panel of Fig. 1, which reports in a colormap the average scale-height of the rest-mass density $\lambda_\rho := \rho/(\nabla\rho) \approx \sqrt{(\rho/\partial_x\rho)^2 + (\rho/\partial_z\rho)^2}$; clearly, the large dominance of the dark-blue color in the low-density regions outside the core of the HMNS, where the low conductivity of matter may induce resistive-MHD effects, indicates that $\lambda_\rho \gtrsim \mathcal{O}(10 \text{ km})$ there.

The right panel in Fig. 1 shows the magnitude of the magnetic field, which shows a filament structure with small-scale variations having characteristic lengthscale of the order of kilometres. Interestingly, even in the lowest-density regions, where the rest-mass density is quite uniform, there are significant structures in the field, indicating substantial variations over the lengthscale of kilometres. This is shown in the lower part of the right panel of Fig. 1, which reports the average scale-height of the magnetic field $\lambda_B := B/(\nabla B) \approx \sqrt{(B/\partial_x B)^2 + (B/\partial_z B)^2}$; clearly, in this case, $\lambda_B \gtrsim \mathcal{O}(1 \text{ km})$ in the low-density regions.

In summary, ideal-MHD simulations generically indicate that: (a) the characteristic lengthscales over which magnetic-field variations can be significant are of the order of 1 km or less, with the lower limit on this scale obviously given by the resolution of the simulation; (b) the characteristic lengthscales over which the rest-mass density variations in the low-density regions can be significant are of the order of 10 km. The density of matter is approximately constant over the lengthscales of variation of the magnetic field; (c) the characteristic timescales relevant for the simulations are of the order of 10 ms. These considerations now motivate our assessment of conditions of applicability of ideal MHD that we will provide next and substantiate some of the approximations we will adopt.

3 Ohmic and Hall timescales

The electrical conductivity of dense matter in neutron stars was studied extensively in the cold regime for temperatures $T \leq 0.1$ MeV which are relevant for isolated neutron stars and neutron stars in X-ray binaries [41, 42, 43, 44, 45, 46, 47, 48, 49, 50]; for a review see [51]. In this regime, the matter is strongly degenerate and the ionic component is solidified, *i.e.*, the electrons are scattered by phonons and impurities. The

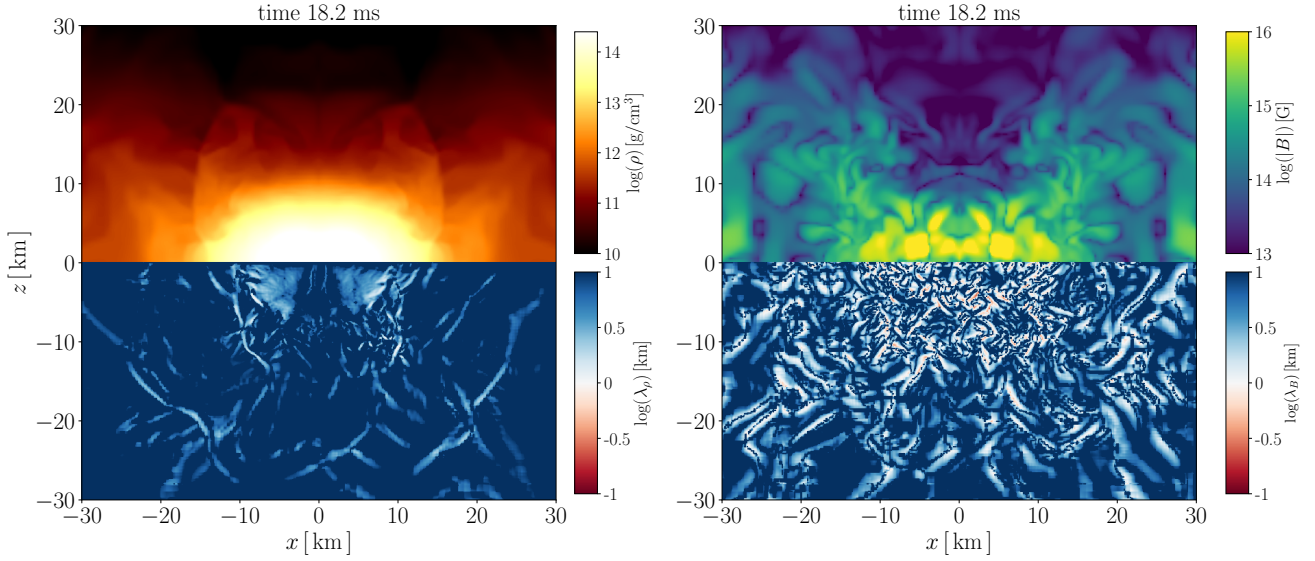


Fig. 1. Two-dimensional cuts in the (x, z) plane of the rest-mass density ρ (left panel) and of the modulus of the magnetic field $|B| = (B_i B^i)^{1/2}$ (right panel); the snapshots refer to $t - t_{\text{mg}} \approx 14.7$ ms of a representative magnetized binary. Shown in the lower parts of the two panels are the scale-heights of the two quantities, $\lambda_\rho \approx \sqrt{(\rho/\partial_x \rho)^2 + (\rho/\partial_z \rho)^2}$ and $\lambda_B \approx \sqrt{(B/\partial_x B)^2 + (B/\partial_z B)^2}$; note that $\lambda_\rho = O(10$ km) and $\lambda_B = O(1$ km), on average.

physical properties of the product of the merger, which may form a long-lived but unstable configuration, differ markedly from ordinary neutron stars; for example, the temperatures are of the order of some tens of MeV ($\sim 10^{11}$ K) [13, 52, 53, 54]. Furthermore, their differential rotation may lead to additional dissipative heating of the post-merger object before it loses its stability and collapses into a black hole [55, 52].

The conductivity tensor in a magnetic field for applications to neutron star mergers was obtained recently [22, 56]. This study provides the conductivity tensor for temperatures extending up to $T \approx 10$ MeV, rest-mass densities down to $\rho \approx 10^6$ g cm $^{-3}$ and for non-quantizing magnetic field $B \leq 10^{14}$ G. In particular, the anisotropy in the conduction due to the field, *i.e.*, the tensor structure of the conductivity was taken fully into account.

Now we turn to the derivation of the time- and lengthscales of interest in terms of the conductivity of matter. As is well-known, the MHD description of low-frequency phenomena in neutron stars is based on the following Maxwell equations

$$\nabla \times \mathbf{E} = -\frac{1}{c} \frac{\partial \mathbf{B}}{\partial t}, \quad \nabla \times \mathbf{B} = \frac{4\pi}{c} \mathbf{j}, \quad (1)$$

where we assume that the magnetic permeability of matter is unity and neglect the displacement current. The system of equations (1) should be closed by Ohm's law for the electric current \mathbf{j} . In the presence of a strong magnetic field, the conduction in neutron star crusts is anisotropic and Ohm's law should be written in a tensor form, *i.e.*, $\mathbf{j} = \hat{\sigma} \mathbf{E}$, where $\hat{\sigma}$ is the electrical conductivity tensor. Substituting the current in the second equation of (1) according to Ohm's law and eliminating the electric field \mathbf{E} , we obtain the induction equation, which describes the magnetic-field evolution as

$$\frac{\partial \mathbf{B}}{\partial t} = -\nabla \times (\hat{\sigma} \nabla \times \mathbf{B}), \quad (2)$$

where $\hat{\sigma}$ is the electrical resistivity tensor (or magnetic viscosity tensor) and is simply the inverse of the electrical conductivity tensor, *i.e.*, $\hat{\sigma} = (c^2/4\pi)\hat{\sigma}^{-1}$.

3.1 Isotropic conductivity tensor

In the case of isotropic conduction $\hat{\sigma}_{ij} = \delta_{ij}\sigma = \text{const.}$, and Eq. (2) reduces to

$$\frac{4\pi}{c^2} \frac{\partial \mathbf{B}}{\partial t} = -\nabla \times \left(\frac{\nabla \times \mathbf{B}}{\sigma} \right). \quad (3)$$

If, as found in Sec. 2, the characteristic lengthscales of variation of the magnetic field are smaller than the lengthscales over which the rest-mass density varies and since σ is a function of the rest-mass density, we can approximate σ as constant over the scale height of the magnetic field. We stress that the validation of this approximation is based on fully dynamical ideal-MHD simulations of binary neutron star mergers described in Sec. 2. Then, upon taking into account that $\nabla \times (\nabla \times \mathbf{B}) = \nabla(\nabla \cdot \mathbf{B}) - \Delta \mathbf{B}$ and $\nabla \cdot \mathbf{B} = 0$, we obtain from Eq. (3)

$$\frac{4\pi\sigma}{c^2} \frac{\partial \mathbf{B}}{\partial t} = \Delta \mathbf{B}. \quad (4)$$

A qualitative estimate of the magnetic field decay timescale τ_d now can be obtained from Eq. (4) if we approximate $|\Delta \mathbf{B}| \approx B/\lambda_B^2$ and $|\partial \mathbf{B}/\partial t| \approx B/\tau_d$. From these estimates, we find that the magnetic field decay (or diffusion) timescale due to Ohmic dissipation is given by the well-known expression

$$\tau_d = \frac{4\pi\sigma\lambda_B^2}{c^2}. \quad (5)$$

3.2 Anisotropic conductivity tensor

The electrical conductivity tensor in the presence of a strong magnetic field can be decomposed as

$$\sigma_{kj} = \delta_{kj}\sigma_0 - \epsilon_{kjm}b_m\sigma_1 + b_k b_j \sigma_2, \quad (6)$$

where $b_k = B_k/B$. Inverting Eq. (6) we find for $\hat{\rho}$

$$\rho_{ik} = \delta_{ik}\rho_0 + \epsilon_{ikm}b_m\rho_1 + b_i b_k \rho_2, \quad (7)$$

where its components are given by

$$\rho_0 = \frac{c^2}{4\pi} \frac{\sigma_0}{\sigma_0^2 + \sigma_1^2}, \quad \rho_1 = \frac{c^2}{4\pi} \frac{\sigma_1}{\sigma_0^2 + \sigma_1^2}, \quad (8)$$

$$\rho_2 = \frac{c^2}{4\pi\sigma} \frac{\sigma_1^2 - \sigma_0\sigma_2}{\sigma_0^2 + \sigma_1^2}, \quad (9)$$

where $\sigma = \sigma_0 + \sigma_2$ is the longitudinal conductivity, *i.e.*, the electrical conductivity in the absence of magnetic field. If the magnetic field is directed along the z axis, then the tensors $\hat{\sigma}$ and $\hat{\rho}$ have the form

$$\hat{\sigma} = \begin{pmatrix} \sigma_0 & -\sigma_1 & 0 \\ \sigma_1 & \sigma_0 & 0 \\ 0 & 0 & \sigma \end{pmatrix}, \quad (10)$$

$$\hat{\rho} = \frac{c^2}{4\pi} \frac{1}{\sigma_0^2 + \sigma_1^2} \begin{pmatrix} \sigma_0 & \sigma_1 & 0 \\ -\sigma_1 & \sigma_0 & 0 \\ 0 & 0 & (\sigma_0^2 + \sigma_1^2)/\sigma \end{pmatrix}. \quad (11)$$

In fact, one can write down Drude-type formulas for each of the three components of the conductivity tensor in the cases of degenerate or nondegenerate electrons [22]

$$\sigma = \frac{n_e e^2 c^2 \tau}{\varepsilon}, \quad \sigma_0 = \frac{\sigma}{1 + (\omega_c \tau)^2}, \quad (12)$$

$$\sigma_1 = \frac{(\omega_c \tau) \sigma}{1 + (\omega_c \tau)^2} = (\omega_c \tau) \sigma_0. \quad (13)$$

Here n_e is the electron number density, e is the elementary charge, τ is the electron mean collision time [or microscopic relaxation time, see Eqs. (13) and (30) of [22]], $\omega_c := ecB\varepsilon^{-1}$ is the cyclotron frequency, and ε is the characteristic energy-scale of electrons. In the degenerate-electron regime $\varepsilon = \varepsilon_F$, where ε_F is the electron Fermi energy; for nondegenerate electrons, instead, $\varepsilon = 3T/2 + \sqrt{(3T/2)^2 + m^2 c^4}$, where T is the temperature and m is the electron mass [22]. From the last expression we recover the well-known results $\varepsilon = mc^2 + 3T/2$ and $\varepsilon = 3T$ for the nonrelativistic and ultrarelativistic regimes, respectively.

Although the expressions (12) and (13) were derived only for strongly degenerate or nondegenerate electrons, it has been argued, on the basis of full numerical study, that these can be applied also for arbitrary degeneracy if one takes for ε the characteristic (to the regime) energy scale of electrons [22].

The components of the resistivity tensor are related to those of the conductivity tensor by relations (8) and (9); using Eqs. (12) and (13) we obtain the following estimates

$$\rho_0 \simeq \frac{c^2}{4\pi\sigma} \equiv \varrho, \quad (14)$$

$$\rho_1 \simeq \frac{c^2}{4\pi} \frac{\sigma_1}{\sigma\sigma_0} \simeq (\omega_c \tau) \varrho \simeq \frac{cB}{4\pi n_e e}, \quad \rho_2 \simeq 0. \quad (15)$$

We now estimate the right-hand side of Eq. (2) using the matrix (7). Writing

$$(\hat{\rho} \nabla \times \mathbf{B})_i = \rho_0 \epsilon_{ijl} \partial_j B_l - \rho_1 (b_i \partial_i B_l - b_j \partial_j B_i) + \rho_2 b_i b_k \epsilon_{kjl} \partial_j B_l, \quad (16)$$

and approximating again $\partial_i B \simeq B/\lambda_B$ and using expressions (14) and (15), we arrive at

$$|\hat{\rho} \nabla \times \mathbf{B}| \simeq \max(1, \omega_c \tau) \varrho \frac{B}{\lambda_B}. \quad (17)$$

In the case of small magnetic field $\omega_c \tau \ll 1$ and we recover the isotropic case from Eq. (2). The evolution of magnetic field is then determined by the Ohmic diffusion timescale τ_d given by Eq. (5). Conversely, in the strongly anisotropic regime, where $\omega_c \tau \gg 1$, the magnetic field evolution is determined by the characteristic timescale τ_B given by

$$\tau_B = \frac{\tau_d}{\omega_c \tau} = \frac{4\pi n_e e \lambda_B^2}{cB} = \frac{4\pi e \rho \lambda_B^2}{cB} \frac{Z}{Am_n}, \quad (18)$$

which follows from Eqs. (2), (5), (15) and (17). In the last step, we used the condition of the charge neutrality, which implies $n_e = Z\rho/(Am_n)$, where Z and A are the charge and the mass number of nuclei, respectively, and m_n is the atomic mass unit.

Thus, in the strongly anisotropic regime (which is realized for sufficiently high magnetic field and low rest-mass densities) the characteristic timescale over which the magnetic field evolves is reduced by a factor of $\omega_c \tau$ due to the Hall effect. We see from Eq. (18), that the timescale τ_B decreases with an increase of the magnetic field and is independent of the electrical conductivity σ (and, consequently, also of the temperature), which is in contrast to the Ohmic diffusion timescale τ_d . The physical reason for this difference lies in the fact that the Hall effect *per-se* is not dissipative. Note however that it can act to facilitate Ohmic dissipation. For instance, the Hall effect may cause the fragmentation of magnetic-field into smaller structures through the Hall instability, which can then accelerate the decay of the field via standard Ohmic dissipation [see [23, 24] and references therein.]

3.3 Estimating magnetic field decay timescale

In order to estimate the Ohmic diffusion timescale given by Eq. (5) we use the following fit formula for the electrical conductivity $\sigma = \sigma(\rho, T, Z)$ [22]

$$\sigma = \frac{1.5 \times 10^{22}}{Z} \left(\frac{T_F}{1 \text{ MeV}} \right)^a \left(\frac{T}{T_F} \right)^{-b} \left(\frac{T}{T_F} + d \right)^c \text{ s}^{-1}, \quad (19)$$

where T and T_F are the temperature of the stellar matter and the Fermi temperature of electrons, respectively. While more accurate tables are available [56], the expression above is accurate up to 10%, which exceeds the accuracy required for our qualitative estimates. The rest-mass density dependence of σ is via the Fermi temperature given by $T_F = 0.511 [\sqrt{1 + (Z\rho_6/A)^{2/3}} - 1] \text{ MeV}$, where $\rho_6 := \rho/(10^6 \text{ g cm}^{-3})$. The fitting parameters

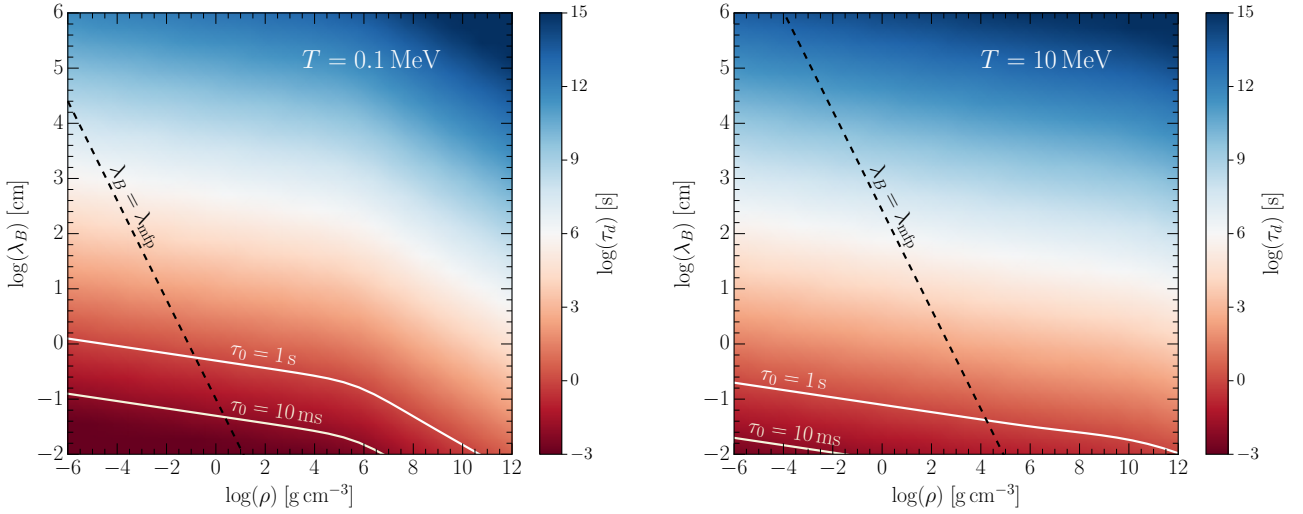


Fig. 2. Dependence of the magnetic-field decay timescale τ_d on the rest-mass density and the typical scale-height of the magnetic field λ_B for $T = 0.1 \text{ MeV} \sim 1.2 \times 10^9 \text{ K}$ (left panel) and $T = 10 \text{ MeV} \sim 1.2 \times 10^{11} \text{ K}$ (right panel). The solid lines correspond to typical timescales of $\tau_0 = 10 \text{ ms}$ and $\tau_0 = 1 \text{ s}$, respectively. The region with $\lambda_B \geq \lambda_{\text{mfp}}$ and $\tau_d \leq \tau_0$ is where the Ohmic dissipation becomes important. The dashed lines show where λ_B becomes equal to the electron mean free path $\lambda_{\text{mfp}}(\rho, T)$; below these lines the MHD description breaks down.

a, b, c, d depend on the charge number of the nucleus via the formulas [57]

$$a(Z) = 0.924 - 0.009 \log Z + 0.003 \log^2 Z, \quad (20)$$

$$b(Z) = 0.507 - 0.028 \log Z - 0.025 \log^2 Z, \quad (21)$$

$$c(Z) = 1.295 - 0.018 \log Z - 0.022 \log^2 Z, \quad (22)$$

$$d(Z) = 0.279 + 0.056 \log Z + 0.035 \log^2 Z. \quad (23)$$

Below, we are interested mainly in the low-density regime of stellar matter, where low values of conductivity could render resistive and Hall effects important. At such low densities, the matter consists mainly of hydrogen or helium nuclei.

Assuming now for simplicity $Z = A = 1$ and using Eqs. (19)–(23) we find an approximation for Eq. (5)

$$\begin{aligned} \tau_d(\rho, T) \simeq & 2.1 \times 10^{12} \left(\frac{T_F}{1 \text{ MeV}} \right) \left(\frac{T}{T_F} \right)^{-0.5} \\ & \times \left(\frac{T}{T_F} + 0.28 \right)^{1.3} \left(\frac{L}{1 \text{ km}} \right)^2 \text{ s}. \end{aligned} \quad (24)$$

We will use this equation to obtain the low-density estimate below, see Eq. (25).

4 Numerical results

We start our discussion with the applicability of the ideal-MHD approximation under conditions relevant for the binary neutron star merger simulations by comparing τ_d with τ_0 . To set a lower limit for the former, we need to choose values for the rest-mass density and the temperature bearing in mind the values encountered in numerical simulations. More specifically, choosing a rest-mass density still compatible with the hydrodynamic description $\rho_6 \lesssim 1$ (see discussion below), and a temperature in

this regime $T \gtrsim 1 \text{ MeV}$, we find $T_F \simeq 0.25 \rho_6^{2/3} \text{ MeV} \ll T$, therefore from Eq. (24) we find an estimate

$$\tau_d \simeq 5 \times 10^{11} \left(\frac{\rho}{1 \text{ g cm}^{-3}} \right)^{0.1} \left(\frac{T}{1 \text{ MeV}} \right)^{0.8} \left(\frac{\lambda_B}{1 \text{ km}} \right)^2 \text{ s}, \quad (25)$$

which is clearly much larger than the typical timescales $\tau_0 = 10 \text{ ms}$ involved in a merger. Given the current limitations on the resolution to the order of a meter and choosing the most favorable temperature and density values we can obtain an effective lower limit on τ_d by substituting in Eq. (25) $\lambda_B = 1 \text{ m}$, $\rho \simeq 10^{-3} \text{ g cm}^{-3}$, and $T = 0.1 \text{ MeV}$, in which case $\tau_d \sim 10^4 \text{ s}$. This value effectively sets a lower limit for τ_d for the adopted resolution scale and is still much larger than τ_0 ¹. Thus, our analysis suggests that resistive effects do not play an important role in the MHD phenomenology of binary neutron star mergers and the ideal-MHD approximation is applicable in the entire parameter range of interest. Our conclusion is in contrast with the previous paradigm of onset of dissipative MHD in low-density regime [18, 21] where the nearly zero-conductivity of matter would have implied $\tau_d \rightarrow 0$.

Figure 2 displays the timescale τ_d in a broad range of the rest-mass density (including the extremely dilute regime relevant for the stellar atmosphere) and the typical lengthscale of magnetic field structures for two values of the temperature. It is seen that at the currently available resolution scale the ideal MHD is applicable in most of the density-temperature range. The dissipative effect would become important only if the resolution is increased by at least several orders of magnitude.

We can make similar considerations also for the timescale τ_B associated with the Hall effect, in which case we can express

¹ Smaller rest-mass densities can be reached in binary mergers, but for $\lambda_B = 1 \text{ m}$ and $T = 0.1 \text{ MeV}$ the MHD approach breaks down already at $\rho \lesssim 10^{-3} \text{ g cm}^{-3}$; see the discussion in Sec. 4.1.

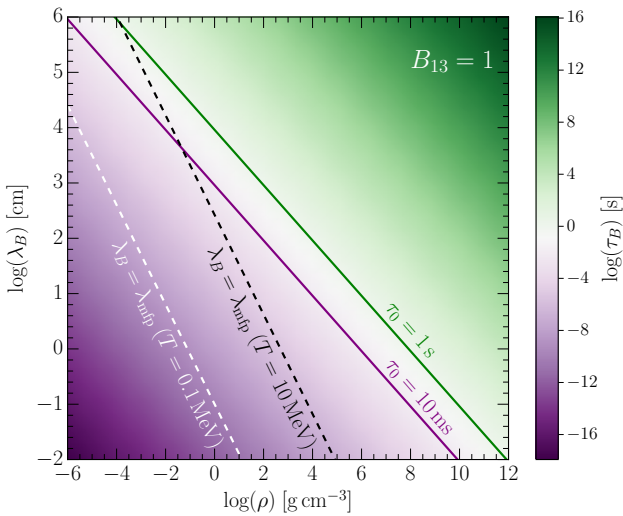


Fig. 3. Dependence of the Hall timescale τ_B on the rest-mass density and the typical scale-height of the magnetic field λ_B . The solid lines correspond to typical timescales of $\tau_0 = 10$ ms and $\tau_0 = 1$ s, respectively. The region with $\lambda_B \geq \lambda_{\text{mfp}}$ and $\tau_B \leq \tau_0$ is where the Hall effect becomes important. The dashed lines show where $\lambda_B = \lambda_{\text{mfp}}(\rho, T)$ for $T = 0.1$ MeV and $T = 10$ MeV; below these lines the MHD description breaks down.

Eq. (18) as

$$\tau_B \approx 1.2 \times 10^2 \times B_{13}^{-1} \left(\frac{\rho}{1 \text{ g cm}^{-3}} \right) \left(\frac{\lambda_B}{1 \text{ km}} \right)^2 \text{ s}, \quad (26)$$

where $B_{13} := B/(10^{13} \text{ G})$. Clearly, the Hall timescale τ_B is much shorter than the diffusion times and it can be in the relevant range of milliseconds for low densities and large magnetic field. The transition from the dissipation regime to the Hall diffusion regime, namely, when the condition $\tau_B < \tau_d$ is fulfilled, occurs at densities $\rho \lesssim 10^{11} B_{13} \text{ g cm}^{-3}$ and is independent of the lengthscale, since both timescales are proportional to λ_B^2 .

The dependence of τ_B on the rest-mass density and λ_B is shown in Fig. 3 for a fixed value of the magnetic field $B_{13} = 1$. At low densities, e.g., $\rho \lesssim 10^{10} \text{ g cm}^{-3}$, we have $\tau_B < \tau_d$ for $B_{13} \geq 0.1$. In this region, therefore, the magnetic field can also be subject to the Hall effect, which will change its distribution on a timescale τ_B . As seen in Fig. 3 and from Eq. (26), τ_B reaches the value $\tau_0 = 10$ ms for $\lambda_B = 1$ km at very low densities $\rho \leq 10^{-4} \text{ g cm}^{-3}$, while for $\lambda_B = 1$ m the value $\tau_B = 10$ ms is reached already at the densities $\rho \leq 10^2 \text{ g cm}^{-3}$, in agreement with the scaling $\tau_B \propto \rho \lambda_B^2$.

4.1 Validity of the MHD approach

After having assessed the ranges of validity of ideal MHD, we can now turn to the next natural question: what limits the applicability of the MHD approach in the present context? Clearly, at very low rest-mass densities the mean free path of particles becomes large and the validity of the MHD description of matter itself can break down. We recall that hydrodynamic description of matter breaks down whenever the electron mean free path $\lambda_{\text{mfp}} \geq \lambda_B$.

The mean free path of electrons is defined as $\lambda_{\text{mfp}} = \tau v$, where τ is the mean collision time. For nondegenerate electrons, $v^2 = 3Tc^2/\varepsilon$ so that we obtain [see the first equation in (12)]

$$\lambda_{\text{mfp}} = \frac{\sigma \varepsilon v}{n_e e^2 c^2} = \frac{A m_n \sigma}{Z e^2 c \rho} \sqrt{3T\varepsilon}. \quad (27)$$

In essence, at low rest-mass densities and large temperatures, i.e., for $\rho_6 \ll 1$ and for temperatures $T \gtrsim 1$ MeV, we can obtain a simple estimate for Eq. (27) [the arguments are similar to those leading to Eq. (25)]

$$\lambda_{\text{mfp}} \approx 4.2 \left(\frac{\rho}{1 \text{ g cm}^{-3}} \right)^{-0.9} \left(\frac{T}{1 \text{ MeV}} \right)^{1.8} \text{ cm}, \quad (28)$$

where we approximated $\varepsilon \approx 3T$. Now we can rewrite the condition of applicability of MHD description, i.e., $\lambda_{\text{mfp}} \leq \lambda_B$, as

$$\rho \gtrsim 1.4 \times 10^{-5} \left(\frac{T}{1 \text{ MeV}} \right)^2 \left(\frac{\lambda_B}{1 \text{ km}} \right)^{-1.1} \text{ g cm}^{-3}. \quad (29)$$

It follows that the higher the temperature or the smaller the typical lengthscale λ_B , the higher the rest-mass density below which the MHD description breaks down. In Figs. 2 and 3 we show with dashed lines where this happens, i.e., where $\lambda_B = \lambda_{\text{mfp}}(\rho, T)$, for two values of the temperature.

Figure 4 shows the regions of validity of the MHD description of matter in the temperature-density plane for $\lambda_B = 1$ km and $\lambda_B = 1$ m, assuming matter as being composed of hydrogen (the case of matter composed of iron is discussed below). The temperature range considered is limited from below by the solidification of matter and covers the range $-1.5 \leq \log(T) \leq 2$. The low-temperature and high-density region corresponds to the regime where ideal MHD conditions are fulfilled. Adjacent to this, a lower density region emerges where the MHD is applicable, but the Hall effect should be taken into account; the exact location of this region depends on the strength of the magnetic field. It moves to lower rest-mass densities for the weaker magnetic field. Above the separation line $\lambda_{\text{mfp}} = \lambda_B$ (solid black line in Fig. 4), the low-density and high-temperature region features matter in the non-hydrodynamic regime, i.e., in a regime where the MHD approximation breaks down and a kinetic approach based on the Boltzmann equation is needed [for a discussion of kinetic regime in the context of relativistic MHD see [58]].

We note that due to the constraint on the rest-mass density given by Eq. (29), the decay timescale τ_d is bounded from below by

$$\tau_d \gtrsim 3.3 \times 10^5 \left(\frac{T}{1 \text{ MeV}} \right) \left(\frac{\lambda_B}{1 \text{ m}} \right)^{1.9} \text{ s}. \quad (30)$$

Assuming now that the merger process is characterized by extremely low values of λ_B and T , e.g., $\lambda_B = 0.1$ m and $T = 0.01$ MeV, we find from Eq. (29) that the MHD description is valid down to a rest-mass density $\rho_{\text{min}} \approx 3.5 \times 10^{-5} \text{ g cm}^{-3}$. In this case, Eq. (30) gives an estimate $\tau_d \approx 40$ s, which is still two orders of magnitude larger than the typical timescale $\tau_0 \sim 10$ ms. Hence, we conclude, that *the ideal-MHD approximation in binary neutron-star simulations is always justified as long*

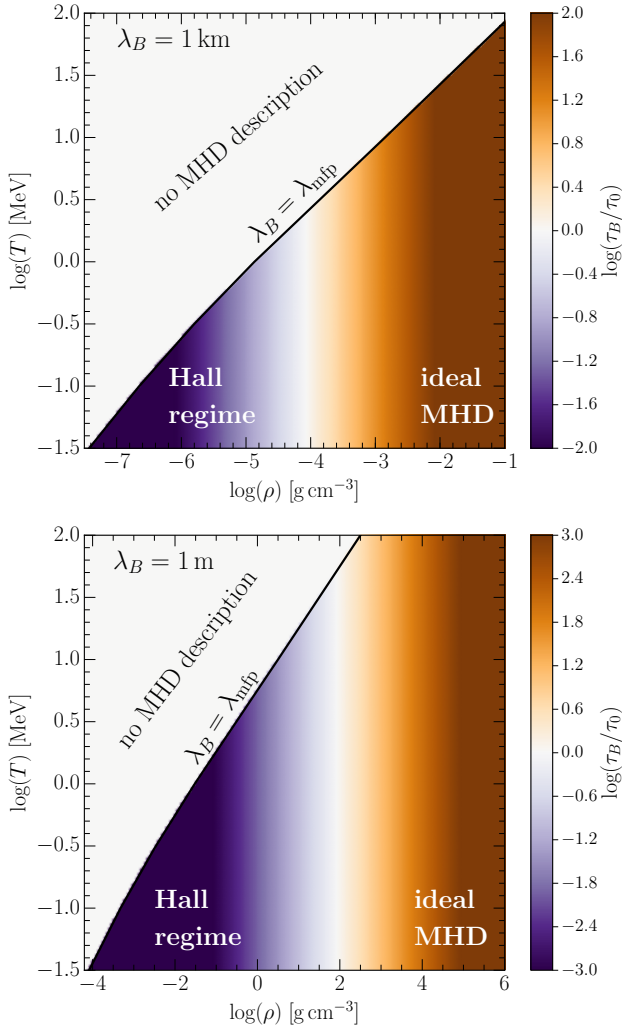


Fig. 4. Regions of the validity of MHD and ideal MHD on the temperature-density plane for two values of the magnetic-field scale-height $\lambda_B = 1$ km (upper panel), and $\lambda_B = 1$ m (lower panel). Areas shaded in dark-orange are the regions where the ideal-MHD approximation holds; areas shaded in dark-violet are the regions where the Hall effect becomes important. The value of the magnetic field is fixed at $B_{13} = 1$, and the typical timescale is taken $\tau_0 = 10$ ms. Above the solid line $\lambda_B = \lambda_{\text{mfp}}$ the MHD description breaks down.

as the MHD description itself is valid. Again, we stress that our conclusion is in contrast to the existing paradigm of modelling the conductivities in neutron star binary mergers, where low-density matter features low conductivity and requires dissipative MHD treatment.

In closing, we ask the inverse question: given that the merger process is characterized by the timescale $\tau_0 = 10$ ms, at what characteristic scales, λ_{im} , do resistive effects become important? To answer this question, we consider $\tau_d \lesssim 10$ ms in Eq. (30) to obtain

$$\lambda_{\text{im}} \simeq 0.1 \left(\frac{T}{1 \text{ MeV}} \right)^{-0.5} \text{ mm}. \quad (31)$$

Thus, in order for resistive effects to be relevant on the typical timescales of the order of 10 ms and for typical temperatures $T \gtrsim 1$ MeV, the characteristic lengthscales of the problem should be of the order of (or less than) a tenth of a millimeter.

For completeness, we also comment on how our estimates will change if the matter consists of heavier elements, *e.g.*, iron nucleus, which has $Z = 26$. As seen from Eqs. (5), [see Eqs. (19)–(23)], the Z -dependence in the timescale τ_d arises mainly from the scaling $\tau_d \propto Z^{-1}$. As a result, in the case of matter composed mainly of iron, τ_d will be reduced roughly by an order of magnitude. On the other hand, the Hall timescale τ_B depends on the type of nuclei as $\tau_B \propto Z/A \simeq 0.5$ for $Z > 1$ [see Eq. (18)]. Hence, τ_B is smaller by a factor of two in the case of iron when compared to hydrogen and our arguments on the applicability of ideal MHD remain qualitatively valid also when $Z = 26$.

5 Conclusions

The multimessenger astronomy era started with the observations of GW170817 in electromagnetic and gravitational waves. Such events, among many other implications, already place constraints on properties of compact star integral parameters, such as masses, radii, and deformability [59, 60, 61, 62, 63, 64, 65, 66] and further insights in various aspects of compact stars are anticipated. In parallel to these developments, the assessment of the transport and dissipation in these events has been brought into focus of microphysics research recently [25, 22].

Motivated by these recent developments, we addressed in this work the role of dissipative processes in the MHD description of neutron star binary mergers. Using recently obtained conductivities of warm plasma in the low-density matter, we have analysed the timescales for the evolution of the magnetic field under the conditions which are relevant for binary neutron-star mergers. We found that the magnetic-field decay time is much larger than the relevant timescales for the merger process in the entire density-temperature range characteristic for these processes. In other words, the ideal MHD approximation is applicable throughout the entire processes of the merger. This conclusion holds for lengthscales down to a meter, which is at least an order of magnitude smaller than currently feasible computational grids. Our finding implies a paradigm shift in resistive MHD treatment of binary neutron star mergers, as these were based on the modeling of conductivities which vanish in the low-density limit [21]. We have demonstrated that the ideal MHD description does not break down due to the onset of dissipation, rather it becomes inapplicable when the hydrodynamic description of matter becomes invalid.

We have demonstrated that the Hall effect plays an important role in the low-density and low-temperature regime. Thus, the ideal MHD description must be supplemented by an approach which takes into account the anisotropy of the fluid via the Hall effect. As is well-known, the Hall effect can act as a mechanism of rearrangement of the magnetic field resulting in resistive instabilities [23, 24].

While our study suggests that the ideal MHD is valid for the binary neutron star simulations, a definitive answer can be reached only through fully numerical studies which include all possible dissipative effects, namely, finite electrical and thermal conductivities, as well as shear and bulk viscosities. Luck-

ily, observations from merging binary neutron stars in the coming years will also provide useful information to resolve this issue.

Special relativistic dissipative MHD formulations including the full anisotropy of the transport coefficients in magnetic fields were developed previously [67, 68, 69]. A general-relativistic formulation of the binary neutron star merger problem which includes the anisotropies of the electrical conductivity has been given already by [21]. We hope that our study will stimulate simulations which will include these effects.

Acknowledgements

AH acknowledges support from the HGS-HIRe graduate program at Goethe University, Frankfurt. AN is supported by an Alexander von Humboldt Fellowship. AS is supported by the Deutsche Forschungsgemeinschaft (Grant No. SE 1836/4-1). Support comes also in part from “NewCompStar” and “PHAROS” COST Actions MP1304 and CA16214; LOEWE-Program in HIC for FAIR; European Union’s Horizon 2020 Research and Innovation Programme (Grant 671698) (call FETHPC-1-2014, project ExaHyPE), the ERC Synergy Grant “BlackHoleCam: Imaging the Event Horizon of Black Holes” (Grant No. 610058). The simulations were performed on the SuperMUC cluster at the LRZ in Garching, on the LOEWE cluster in CSC in Frankfurt, on the HazelHen cluster at the HLRS in Stuttgart.

References

1. LIGO SCIENTIFIC COLLABORATION AND VIRGO COLLABORATION collaboration, The LIGO Scientific Collaboration and The Virgo Collaboration, *Gw170817: Observation of gravitational waves from a binary neutron star inspiral*, *Phys. Rev. Lett.* **119** (Oct, 2017) 161101.
2. LIGO Scientific Collaboration, Virgo Collaboration, F. Gamma-Ray Burst Monitor and INTEGRAL, *Gravitational waves and gamma-rays from a binary neutron star merger: Gw170817 and grb 170817a*, *Astrophys. J. Lett.* **848** (2017) L13, [1710.05834].
3. LIGO SCIENTIFIC COLLABORATION AND VIRGO COLLABORATION collaboration, The LIGO Scientific Collaboration, the Virgo Collaboration, B. P. Abbott, R. Abbott, T. D. Abbott, F. Acernese et al., *Multi-messenger observations of a binary neutron star merger*, *Astrophys. J. Lett.* **848** (2017) L12.
4. B. P. Abbott, R. Abbott, T. D. Abbott, F. Acernese, K. Ackley, C. Adams et al., *Estimating the Contribution of Dynamical Ejecta in the Kilonova Associated with GW170817*, *Astrophys. J. Lett.* **850** (Dec., 2017) L39, [1710.05836].
5. D. A. Coulter, R. J. Foley, C. D. Kilpatrick, M. R. Drout, A. L. Piro, B. J. Shappee et al., *Swope Supernova Survey 2017a (SSS17a), the optical counterpart to a gravitational wave source*, *Science* **358** (Dec., 2017) 1556–1558, [1710.05452].
6. S. Smartt, T. Chen and et al., *A kilonova as the electromagnetic counterpart to a gravitational-wave source*, *Nature* **551** (Nov., 2017) 75–79, [1710.05841].
7. B. P. Abbott, R. Abbott, T. D. Abbott, F. Acernese, K. Ackley, C. Adams et al., *A gravitational-wave standard siren measurement of the Hubble constant*, *Nature* **551** (Nov., 2017) 85–88, [1710.05835].
8. J. A. Faber and F. A. Rasio, *Binary neutron star mergers*, *Living Rev. Relativity* **15** 8 (2012).
9. V. Paschalidis, *General relativistic simulations of compact binary mergers as engines for short gamma-ray bursts*, *Classical and Quantum Gravity* **34** (Apr., 2017) 084002, [1611.01519].
10. L. Baiotti and L. Rezzolla, *Binary neutron-star mergers: a review of Einstein’s richest laboratory*, *Rept. Prog. Phys.* **80** (2017) 096901, [1607.03540].
11. L. Rezzolla, B. Giacomazzo, L. Baiotti, J. Granot, C. Kouveliotou and M. A. Aloy, *The Missing Link: Merging Neutron Stars Naturally Produce Jet-like Structures and Can Power Short Gamma-ray Bursts*, *Astrophys. J. Letters* **732** (May, 2011) L6, [1101.4298].
12. K. Kiuchi, K. Kyutoku, Y. Sekiguchi, M. Shibata and T. Wada, *High resolution numerical relativity simulations for the merger of binary magnetized neutron stars*, *Phys. Rev. D* **90** (Aug., 2014) 041502, [1407.2660].
13. C. Palenzuela, S. L. Liebling, D. Neilsen, L. Lehner, O. L. Caballero, E. O’Connor et al., *Effects of the microphysical equation of state in the mergers of magnetized neutron stars with neutrino cooling*, *Phys. Rev. D* **92** (Aug., 2015) 044045, [1505.01607].
14. T. Kawamura, B. Giacomazzo, W. Kastaun, R. Ciolfi, A. Endrizzi, L. Baiotti et al., *Binary neutron star mergers and short gamma-ray bursts: Effects of magnetic field orientation, equation of state, and mass ratio*, *Phys. Rev. D* **94** (Sept., 2016) 064012, [1607.01791].
15. M. Ruiz, R. N. Lang, V. Paschalidis and S. L. Shapiro, *Binary Neutron Star Mergers: A Jet Engine for Short Gamma-Ray Bursts*, *Astrophys. J. Lett.* **824** (June, 2016) L6, [1604.02455].
16. K. Kiuchi, K. Kyutoku, Y. Sekiguchi and M. Shibata, *Global simulations of strongly magnetized remnant massive neutron stars formed in binary neutron star mergers*, *arXiv:1710.01311* (Oct., 2017), [1710.01311].
17. M. Ruiz, S. L. Shapiro and A. Tsokaros, *GW170817, general relativistic magnetohydrodynamic simulations, and the neutron star maximum mass*, *Phys. Rev. D* **97** (Jan., 2018) 021501, [1711.00473].
18. K. Dionysopoulou, D. Alic, C. Palenzuela, L. Rezzolla and B. Giacomazzo, *General-relativistic resistive magnetohydrodynamics in three dimensions: Formulation and tests*, *Phys. Rev. D* **88** (Aug., 2013) 044020, [1208.3487].
19. C. Palenzuela, L. Lehner, S. L. Liebling, M. Ponce, M. Anderson, D. Neilsen et al., *Linking electromagnetic and gravitational radiation in coalescing binary neutron stars*, *Phys. Rev. D* **88** (Aug., 2013) 043011, [1307.7372].
20. C. Palenzuela, L. Lehner, M. Ponce, S. L. Liebling, M. Anderson, D. Neilsen et al., *Electromagnetic and Gravitational Outputs from Binary-Neutron-Star Coalescence*, *Phys. Rev. Lett.* **111** (Aug., 2013) 061105, [1301.7074].

21. K. Dionysopoulou, D. Alic and L. Rezzolla, *General-relativistic resistive-magnetohydrodynamic simulations of binary neutron stars*, *Phys. Rev. D* **92** (Oct., 2015) 084064, [[1502.02021](#)].
22. A. Harutyunyan and A. Sedrakian, *Electrical conductivity of a warm neutron star crust in magnetic fields*, *Phys. Rev. C* **94** (Aug., 2016) 025805, [[1605.07612](#)].
23. K. N. Gourgouliatos and R. Hollerbach, *Resistive tearing instability in electron MHD: application to neutron star crusts*, *Mon. Not. R. Astron. Soc.* **463** (Dec., 2016) 3381–3389, [[1607.07874](#)].
24. L. L. Kitchatinov, *Double Hall instability: A catalyzer of magnetic energy release*, *Astronomy Letters* **43** (Sept., 2017) 624–633, [[1705.10077](#)].
25. M. G. Alford, L. Bovard, M. Hanauske, L. Rezzolla and K. Schwenzer, *Viscous dissipation and heat conduction in binary neutron-star mergers*, *Phys. Rev. Lett.* **120** (Jan., 2018) 041101, [[1707.09475](#)].
26. F. Rasio and S. Shapiro, *TOPICAL REVIEW: Coalescing binary neutron stars*, *Class. Quantum Grav.* **16** (June, 1999) R1–R29, [[gr-qc/9902019](#)].
27. E. P. Velikhov, *Sov. Phys. JETP* **9** (1959) 995.
28. S. Chandrasekhar, *The Stability of Non-Dissipative Couette Flow in Hydromagnetics*, *Proc. Natl. Acad. Sci.* **46** (Feb., 1960) 253–257.
29. M. Anderson, E. W. Hirschmann, L. Lehner, S. L. Liebling, P. M. Motl, D. Neilsen et al., *Magnetized Neutron-Star Mergers and Gravitational-Wave Signals*, *Phys. Rev. Lett.* **100** (May, 2008) 191101, [[0801.4387](#)].
30. Y. T. Liu, S. L. Shapiro, Z. B. Etienne and K. Taniguchi, *General relativistic simulations of magnetized binary neutron star mergers*, *Phys. Rev. D* **78** (2008) 024012, [[0803.4193](#)].
31. B. Giacomazzo, L. Rezzolla and L. Baiotti, *Can magnetic fields be detected during the inspiral of binary neutron stars?*, *Mon. Not. R. Astron. Soc.* **399** (Oct., 2009) L164–L168, [[0901.2722](#)].
32. K. Kiuchi, Y. Sekiguchi, M. Shibata and K. Taniguchi, *Long-term general relativistic simulation of binary neutron stars collapsing to a black hole*, *Phys. Rev. D* **80** (Sept., 2009) 064037, [[0904.4551](#)].
33. B. Giacomazzo, L. Rezzolla and L. Baiotti, *Accurate evolutions of inspiralling and magnetized neutron stars: Equal-mass binaries*, *Phys. Rev. D* **83** (Feb, 2011) 044014.
34. K. Kiuchi, P. Cerdá-Durán, K. Kyutoku, Y. Sekiguchi and M. Shibata, *Efficient magnetic-field amplification due to the Kelvin-Helmholtz instability in binary neutron star mergers*, *Phys. Rev. D* **92** (Dec., 2015) 124034, [[1509.09205](#)].
35. D. M. Siegel, R. Ciolfi, A. I. Harte and L. Rezzolla, *Magnetorotational instability in relativistic hypermassive neutron stars*, *Phys. Rev. D* **87** (June, 2013) 121302, [[1302.4368](#)].
36. T. Rembiasz, J. Guilet, M. Obergaulinger, P. Cerdá-Durán, M. A. Aloy and E. Müller, *On the maximum magnetic field amplification by the magnetorotational instability in core-collapse supernovae*, *Mon. Not. R. Astron. Soc.* **460** (Aug., 2016) 3316–3334, [[1603.00466](#)].
37. M. Obergaulinger, M. A. Aloy and E. Müller, *Local simulations of the magnetized Kelvin-Helmholtz instability in neutron-star mergers*, *Astron. Astrophys.* **515** (June, 2010) A30, [[1003.6031](#)].
38. J. Zrake and A. I. MacFadyen, *Spectral and Intermittency Properties of Relativistic Turbulence*, *Astrophys. J.* **763** (Jan., 2013) L12, [[1210.4066](#)].
39. K. Kiuchi, Y. Sekiguchi, K. Kyutoku, M. Shibata, K. Taniguchi and T. Wada, *High resolution magnetohydrodynamic simulation of black hole-neutron star merger: Mass ejection and short gamma ray bursts*, *Phys. Rev. D* **92** (Sept., 2015) 064034, [[1506.06811](#)].
40. Z. B. Etienne, V. Paschalidis, R. Haas, P. Mösta and S. L. Shapiro, *IllinoisGRMHD: an open-source, user-friendly GRMHD code for dynamical spacetimes*, *Class. Quantum Grav.* **32** (Sept., 2015) 175009, [[1501.07276](#)].
41. C. J. Horowitz, D. K. Berry, C. M. Briggs, M. E. Caplan, A. Cumming and A. S. Schneider, *Disordered Nuclear Pasta, Magnetic Field Decay, and Crust Cooling in Neutron Stars*, *Physical Review Letters* **114** (Jan., 2015) 031102, [[1410.2197](#)].
42. N. Itoh, S. Uchida, Y. Sakamoto, Y. Kohyama and S. Nozawa, *The Second Born Corrections to the Electrical and Thermal Conductivities of Dense Matter in the Liquid Metal Phase*, *ApJ* **677** (Apr., 2008) 495–502, [[0708.2967](#)].
43. A. Y. Potekhin, *Electron conduction in magnetized neutron star envelopes*, *A&A* **351** (Nov., 1999) 787–797, [[astro-ph/9909100](#)].
44. D. A. Baiko, A. D. Kaminker, A. Y. Potekhin and D. G. Yakovlev, *Ion Structure Factors and Electron Transport in Dense Coulomb Plasmas*, *Physical Review Letters* **81** (Dec., 1998) 5556–5559, [[physics/9811052](#)].
45. N. Itoh, H. Hayashi and Y. Kohyama, *Electrical and Thermal Conductivities of Dense Matter in the Crystalline Lattice Phase. III. Inclusion of Lower Densities*, *ApJ* **418** (Nov., 1993) 405.
46. N. Itoh and Y. Kohyama, *Electrical and thermal conductivities of dense matter in the crystalline lattice phase. II - Impurity scattering*, *ApJ* **404** (Feb., 1993) 268–270.
47. N. Itoh, Y. Kohyama, N. Matsumoto and M. Seki, *Electrical and thermal conductivities of dense matter in the crystalline lattice phase*, *ApJ* **285** (Oct., 1984) 758–765.
48. R. Nandkumar and C. J. Pethick, *Transport coefficients of dense matter in the liquid metal regime*, *MNRAS* **209** (Aug., 1984) 511–524.
49. S. Mitake, S. Ichimaru and N. Itoh, *Electrical and thermal conductivities of dense matter in the liquid metal phase. II - Low-temperature quantum corrections*, *ApJ* **277** (Feb., 1984) 375–378.
50. N. Itoh, S. Mitake, H. Iyetomi and S. Ichimaru, *Electrical and thermal conductivities of dense matter in the liquid metal phase. I - High-temperature results*, *ApJ* **273** (Oct., 1983) 774–782.
51. A. Schmitt and P. Shternin, *Reaction rates and transport in neutron stars*, *ArXiv e-prints* (Nov., 2017) , [[1711.06520](#)].

52. M. Hanauske, K. Takami, L. Bovard, L. Rezzolla, J. A. Font, F. Galeazzi et al., *Rotational properties of hypermassive neutron stars from binary mergers*, *Phys. Rev. D* **96** (Aug., 2017) 043004, [[1611.07152](#)].
53. W. Kastaun, R. Ciolfi, A. Endrizzi and B. Giacomazzo, *Structure of stable binary neutron star merger remnants: Role of initial spin*, *Phys. Rev. D* **96** (Aug., 2017) 043019, [[1612.03671](#)].
54. L. Bovard, D. Martin, F. Guercilena, A. Arcones, L. Rezzolla and O. Korobkin, *On r-process nucleosynthesis from matter ejected in binary neutron star mergers*, *Phys. Rev. D* **96** (Dec., 2017) 124005, [[1709.09630](#)].
55. W. Kastaun and F. Galeazzi, *Properties of hypermassive neutron stars formed in mergers of spinning binaries*, *Phys. Rev. D* **91** (Mar., 2015) 064027, [[1411.7975](#)].
56. A. Harutyunyan and A. Sedrakian, *Electrical conductivity tensor of dense plasma in magnetic fields*, *PoS MPC2015* (July, 2016) 011, [[1607.04541](#)].
57. A. Harutyunyan, *Relativistic hydrodynamics and transport in strongly correlated systems*. PhD thesis, Goethe University, Frankfurt am Main, Germany, 2017.
58. L. Rezzolla and O. Zanotti, *Relativistic Hydrodynamics*. Oxford University Press, Oxford, UK, 2013. 10.1093/acprof:oso/9780198528906.001.0001.
59. A. Bauswein, O. Just, H.-T. Janka and N. Stergioulas, *Neutron-star Radius Constraints from GW170817 and Future Detections*, *Astrophys. J. Lett.* **850** (Dec., 2017) L34, [[1710.06843](#)].
60. B. Margalit and B. D. Metzger, *Constraining the Maximum Mass of Neutron Stars from Multi-messenger Observations of GW170817*, *Astrophys. J. Lett.* **850** (Dec., 2017) L19, [[1710.05938](#)].
61. D. Radice, *General-relativistic Large-eddy Simulations of Binary Neutron Star Mergers*, *Astrophys. J. Lett.* **838** (Mar., 2017) L2, [[1703.02046](#)].
62. L. Rezzolla, E. R. Most and L. R. Weih, *Using Gravitational-wave Observations and Quasi-universal Relations to Constrain the Maximum Mass of Neutron Stars*, *Astrophys. J. Lett.* **852** (Jan., 2018) L25, [[1711.00314](#)].
63. M. Ruiz, S. L. Shapiro and A. Tsokaros, *GW170817, general relativistic magnetohydrodynamic simulations, and the neutron star maximum mass*, *Phys. Rev. D* **97** (Jan., 2018) 021501, [[1711.00473](#)].
64. M. Shibata, S. Fujibayashi, K. Hotokezaka, K. Kiuchi, K. Kyutoku, Y. Sekiguchi et al., *Modeling GW170817 based on numerical relativity and its implications*, *Phys. Rev. D* **96** (Dec., 2017) 123012, [[1710.07579](#)].
65. V. Paschalidis, K. Yagi, D. Alvarez-Castillo, D. B. Blaschke and A. Sedrakian, *Implications from GW170817 and I-Love-Q relations for relativistic hybrid stars*, *arXiv:1712.00451* (Dec., 2017), [[1712.00451](#)].
66. E. R. Most, L. R. Weih, L. Rezzolla and J. Schaffner-Bielich, *New constraints on radii and tidal deformabilities of neutron stars from GW170817*, *arxiv:1803.00549* (Mar., 2018), [[1803.00549](#)].
67. X.-G. Huang, M. Huang, D. H. Rischke and A. Sedrakian, *Anisotropic hydrodynamics, bulk viscosities, and r-modes of strange quark stars with strong magnetic fields*, *Phys. Rev. D* **81** (Feb., 2010) 045015, [[0910.3633](#)].
68. X.-G. Huang, A. Sedrakian and D. H. Rischke, *Kubo formulas for relativistic fluids in strong magnetic fields*, *Annals of Physics* **326** (Dec., 2011) 3075–3094, [[1108.0602](#)].
69. J. Hernandez and P. Kovtun, *Relativistic magnetohydrodynamics*, *Journal of High Energy Physics* **5** (May, 2017) 1, [[1703.08757](#)].